Sea ice production and water mass modification in the eastern Laptev Sea

T. Krumpen,[1] J. A. Hölemann,[2] S. Willmes,[3] M. A. Morales Maqueda,[4] T. Busche,[5] I. A. Dmitrenko,[6] R. Gerdes,[1] C. Haas,[7] G. Heinemann,[3] S. Hendricks,[1] H. Kassens,[6] L. Rabenstein,[8] and D. Schröder[3]

Received 22 July 2010; revised 5 January 2011; accepted 2 March 2011; published 21 May 2011.

[1] A simple polynya flux model driven by standard atmospheric forcing is used to investigate the ice formation that took place during an exceptionally strong and consistent western New Siberian (WNS) polynya event in 2004 in the Laptev Sea. Whether formation rates are high enough to erode the stratification of the water column beneath is examined by adding the brine released during the 2004 polynya event to the average winter density stratification of the water body, preconditioned by summers with a cyclonic atmospheric forcing (comparatively weakly stratified water column). Beforehand, the model performance is tested through a simulation of a well-documented event in April 2008. Neglecting the replenishment of water masses by advection into the polynya area, we find the probability for the occurrence of density-driven convection down to the bottom to be low. Our findings can be explained by the distinct vertical density gradient that characterizes the area of the WNS polynya and the apparent lack of extreme events in the eastern Laptev Sea. The simple approach is expected to be sufficiently rigorous, since the simulated event is exceptionally strong and consistent, the ice production and salt rejection rates are likely to be overestimated, and the amount of salt rejected is distrusted over a comparatively weakly stratified water column. We conclude that the observed erosion of the halocline and formation of vertically mixed water layers during a WNS polynya event is therefore predominantly related to wind- and tidally driven turbulent mixing processes.

Citation: Krumpen, T., et al. (2011), Sea ice production and water mass modification in the eastern Laptev Sea, *J. Geophys. Res.*, *116*, C05014, doi:10.1029/2010JC006545.

1. Introduction

[2] Numerous coastal polynyas form every winter in all peripheral shelf seas of the central Arctic [*Gloersen et al.*, 1992; *Barber and Massom*, 2007]. These coastal polynyas (also termed flaw polynyas when they form adjacent to landfast ice), are nonlinear-shaped regions of open water and thin ice created as offshore winds push the pack ice away from the coast or the landfast ice edge [*Smith et al.*, 1990; *Morales Maqueda et al.*, 2004]. Surface heat loss within a coastal polynya results in the formation of frazil ice that is transported toward the downwind edge of the polynya. The frazil ice arriving at the polynya edge forms a thin layer of ice and water slurry called grease ice [*Martin and Kauffman*, 1981] which thickens and eventually consolidates as it drifts further offshore. Salt, excluded from the almost pure ice matrix, is first concentrated in the brine situated between the ice crystals. This brine convects as plumes/streamers into the seawater on which the ice floats. The process induces haline convection and erodes the density stratification of the water column [*Ivanov and Golovin*, 2007]. If haline convection is penetrative, dense bottom water may be formed [*Backhaus et al.*, 1997]. Density-driven vertical mixing in coastal polynyas is a key control of the shelf sea dynamics since it affects momentum, heat and biogeochemical air-sea fluxes [*Morales Maqueda et al.*, 2004], and provides conditions for downslope transport of water, sediments and pollutants [*Reimnitz et al.*, 1994; *Sherwood*, 2000; *Smedsrud*, 2004].

[3] In terms of ice production and polynya-induced formation of higher saline water, the Laptev Sea is a controversially discussed circum-Arctic shelf sea [*Zakharov*, 1966; *Cavalieri and Martin*, 1994; *Dethleff et al.*, 1998;

[1]Department of Sea Ice Physics, Alfred Wegener Institute, Bremerhaven, Germany.
[2]Department of Observational Oceanography, Alfred Wegener Institute, Bremerhaven, Germany.
[3]Department of Environmental Meteorology, University of Trier, Trier, Germany.
[4]National Oceanography Centre, Liverpool, UK.
[5]Microwave and Radar Institute, German Aerospace Center, Wesseling, Germany.
[6]Leibniz Institute of Marine Sciences, University of Kiel, Kiel, Germany.
[7]Department of Earth and Atmospheric Sciences, University of Alberta, Edmonton, Alberta, Canada.
[8]Institute of Geophysics, ETH Zurich, Zurich, Switzerland.

0148-0227/11/2010JC006545

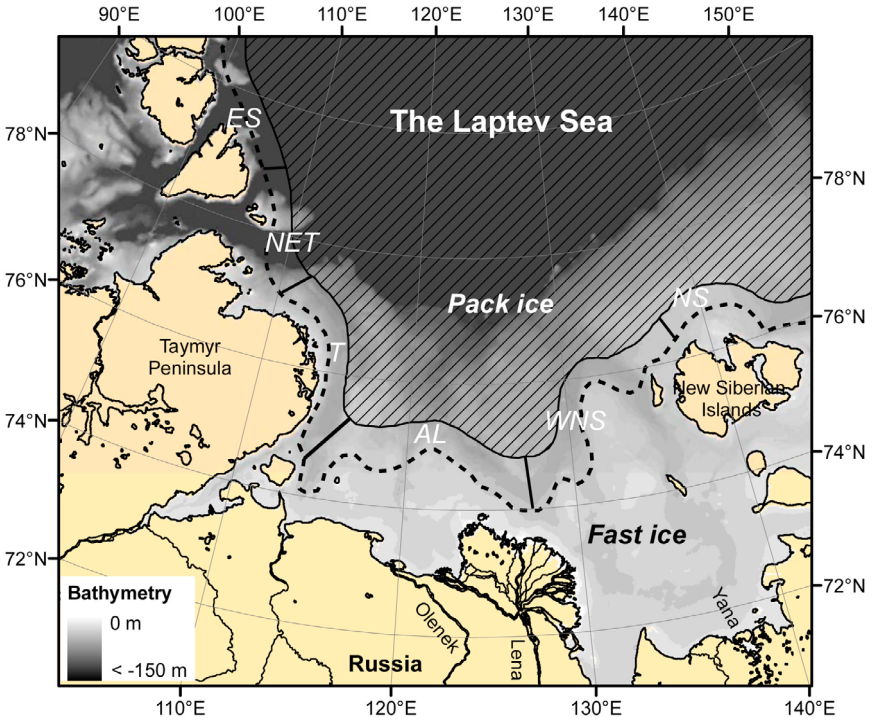

Figure 1. Map of the Laptev Sea showing the three distinct sea ice components: the fast ice zone, the pack ice zone, and the location of the flaw polynyas. The mean lateral extent of the fast ice at the end of the winter is indicated by the black dashed line. The grey shaded area north of the fast ice represents the pack ice zone. Between pack ice and fast ice edge, flaw polynyas are formed. The New Siberian polynya (NS), the western New Siberian polynya (WNS), the Anabar-Lena polynya (AL), the Taymyr polynya (T), the northeastern Taymyr polynya (NET), and the eastern Severnaya Zemlya (ESZ) polynya. Color coding corresponds to the bathymetry (water depth in m, source is *Smith and Sandwell* [1997]).

Dmitrenko et al., 2005, 2009; *Willmes et al.*, 2011; *Dethleff*, 2010]. Constant offshore winds generate a quasi-perennial flaw polynya extending almost 2000 km along the shelf and landfast sea ice several hundreds of kilometers wide. Following *Zakharov* [1966], the prominent flaw polynyas in the Laptev Sea are the New Siberian polynya (NS), the western New Siberian polynya (WNS), the Anabar-Lena polynya (AL), the Taymyr polynya (T), the northeastern Taymyr polynya (NET), and the eastern Severnaya Zemlya polynya (ESZ, compare Figure 1). According to calculations made by *Aagaard et al.* [1985] and *Dmitrenko et al.* [2009], the annual net sea ice production in the entire Laptev Sea amounts to roughly 900 km^3.

[4] Following *Dethleff et al.* [1998], who investigated ice formation in Laptev Sea polynyas by means of a model applied to calculate ocean-to-atmosphere heat flux and the resulting new ice formation over open water, as much as 258 km^3 of ice is produced in polynyas. Putting the results of *Dethleff et al.* [1998] in relation to the annual ice production estimated by *Dmitrenko et al.* [2009], flaw polynyas produce about 26% of the annual Laptev Sea ice. The average annual polynya ice production calculated by *Winsor and Bjoerk* [2000] is far lower. The authors investigated Arctic polynyas during 39 winter seasons from 1958 to 1997 by means of a large-scale polynya model and calculated an average annual ice production of 43 km^3 (4.3% of the annual ice production). Findings made by *Willmes et al.* [2011] are somewhat similar to what is suggested by *Winsor and Bjoerk* [2000]. According to their satellite-based estimates, the annual polynya ice production amounts to 5.5% (55 km^3) of the total seasonal ice production and is hence significantly smaller than approximations made by *Dethleff et al.* [1998]. The large discrepancies that exist in the estimated contribution of Laptev Sea polynyas to the annual net sea ice formation are a consequence of the use of different sensor systems, models, observation periods and alternating definitions for the term "active polynya" [*Krumpen et al.*, 2011a].

[5] Potential sites for dense water formation are located in the central and northwestern Laptev Sea [*Willmes et al.*, 2011; *Dethleff*, 2010]. Dense water formed in these polynyas is believed to feed the Arctic halocline but is found to be insufficiently dense to ventilate the layers below [*Schauer et al.*, 1997; *Lenn et al.*, 2008].

[6] In the eastern Laptev Sea and the area around the WNS polynya (Figure 1), the large summer runoff of the Lena river freshens the surface ocean layer and leads to the development of a distinct vertical density gradient in the water column [*Dmitrenko et al.*, 2005]. The strength of the stratification is controlled by the atmospheric circulation during summer months [*Dmitrenko et al.*, 2008]. Anticyclonic wind conditions force the riverine water northward and result in a stronger density stratification in the eastern Laptev sea. Cyclonic atmospheric circulation deflects the freshwater

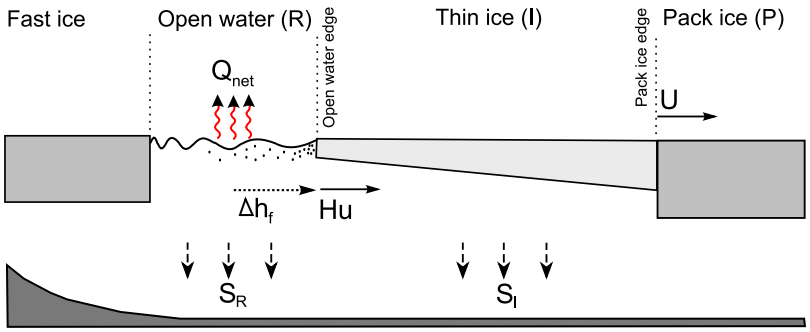

Figure 2. Schematic illustrating of the polynya model. In the open water area, heat loss to the atmosphere (Q_{net}) results in frazil ice growth with rate $\Delta h_f/\Delta_t$. Frazil ice piles up against the open water edge with thickness H and then drifts away from the edge with speed u. The pack ice edge moves with velocity U. The instantaneous salt flux from frazil ice growth in the open water zone is given by S_R. Salt rejection induced by the continuous growth of consolidated new ice is denoted by S_I.

plume of the River Lena eastward toward the East Siberian Sea, thus causing higher salinities in the eastern Laptev Sea and the area around the WNS polynya. This results in weaker density stratification, as observed in 2007 by *Hölemann et al.* [2011] and *Dmitrenko et al.* [2010a].

[7] According to *Dmitrenko et al.* [2005], the probability for the water column to get fully mixed down to the seafloor in the region of the Western New Siberian polynya is around 20%. Their findings are based on hydrological data obtained between1979 and 1999 rather than sea-ice observations. However, owing to the strong stratification and the noticeable lack of extreme polynya events in the Laptev Sea [*Winsor and Bjoerk*, 2000], we argue that ice production alone in the WNS polynya is not high enough to erode the halocline and that the probability for dense water formation is far lower than the 20% calculated by *Dmitrenko et al.* [2005]. In this paper, we therefore investigate the effect of intense ice formation taking place during an exceptionally strong and consistent polynya event on a water column structure with a relatively weak vertical density gradient, preconditioned by a cyclonic atmospheric circulation during summer [*Dmitrenko et al.*, 2010a].

[8] Below we use an idealized polynya flux model [*Pease*, 1987] to simulate an extremely strong opening event of the WNS polynya. The event was chosen based on a time series of Envisat synthetic aperture radar (SAR) images covering a period of 7 winters (2003–2009). Starting on 10 February 2004, constant offshore winds opened up the polynya for a period of 27 days. The flux model computes the evolution of the open water area and resultant thin ice zone, and the associated ice and salt fluxes. In winter 2004, the water body was preconditioned toward a weak stratification state by a cyclonic atmospheric circulation regime during summer 2003. For the calculation presented in this study we use an average water mass structure that is representative of the density stratification in the area of the WNS polynya during years with a cyclonic atmospheric circulation. The underlying hydrographic data are taken from the data archive of the Russian Arctic and Antarctic Research Institute and former Russian-German expeditions. Whether ice formation during the 2004 polynya event is strong enough to erode halocline is judged by integrating the amount of salt rejection over the weakly stratified water column.

[9] Because ice production and salt rejection in a polynya are highest inside the open water zone, an accurate determination of ice and salt fluxes require a correct simulation of the open water edge evolution [*Morales Maqueda et al.*, 2004]. Unfortunately, a satellite-based verification of computed open water extents is difficult, since open water edges are not easily identifiable in satellite images [*Barber et al.*, 2001; *Haarpaintner et al.*, 2001]. Prior to the simulation of the major polynya opening event observed in 2004, we therefore test the model parameterizations and performance by applying it to a minor but well documented opening event in April 2008. The event lasted for approximately 6 days and was observed during the TRANSDRIFT XIII (TD XIII) expedition carried out within the framework of the Russian-German research cooperation programme “Laptev Sea System”. Information on the temporal and spatial evolution of the open water area and pack ice edges, as well as the thickness of thin ice, are obtained from photogrammetric and electromagnetic airborne surveys, thermal infrared satellite imagery and high-resolution RADAR satellites.

[10] The structure of the paper is as follows. First, the model description is given in section 2. We then describe the data set used for model calibration and verification (section 3). In section 4, we apply the model to the well documented event of April 2008 and to the exceptionally strong opening event of February 2004. In addition, the model parameterizations and performance are tested and discussed by comparing simulated open water width and thin ice thickness with observations and satellite-based estimates and by means of a sensitivity study. Subsequently, we investigate the effect of ice production during the 2004 event on a weakly stratified water body, preconditioned by a cyclonic circulation regime in summer (section 5). Conclusions are drawn in section 6.

2. Polynya Flux Model Description

[11] The objective of our model is to calculate the amount of ice production and salt rejection in a flaw polynya on the basis of wind and air temperature information. Below, we briefly describe the concepts behind the model. Following *Haarpaintner et al.* [2001], two simple one-dimensional

drift algorithms are used to simulate the evolutions of the open water region and the pack ice edge (Figure 2).

[12] The first algorithm computes the width of the wind-generated open water zone R [*Pease*, 1987]. Because of its simple idealized formulation and its ability to provide fairly accurate ice production estimates [*Krumpen et al.*, 2011a], a flux model is used. Polynya flux models were first formulated by *Pease* [1987], embracing an idea of *Lebedev* [1968] that wind-generated coastal polynyas attain a maximum size determined by a balance between ice production within and flux of ice out of the open water zone [*Morales Maqueda et al.*, 2004; *Willmott et al.*, 2007; *Krumpen et al.*, 2011a]. Following *Pease* [1987], the width of the open water zone, R, can be expressed as

$$R_t = R_{t-\Delta_t}\left(1 - \Delta h_f / H\right) + u\Delta_t, \quad (1)$$

where R_t is the open water width at time t and Δt is the temporal resolution of the atmospheric data set. Δh_f is the amount of frazil ice produced in the water column between time t and $t - \Delta t$, calculated from the surface heat balance Q_{net} [*Cavalieri and Martin*, 1994]

$$Q_s + Q_l + Q_{lw} + (1 - \alpha)Q_{sw} = -Q_{net}/\left(\rho_f L_s\right) = h_f, \quad (2)$$

where Q_s and Q_l are the turbulent sensible and latent heat fluxes, respectively. Q_{lw} is the net longwave radiation at the sea surface, Q_{sw} is the shortwave solar radiation, and α is the surface albedo [*Cavalieri and Martin*, 1994; *Morales Maqueda et al.*, 2004]. In (2), ρ_f is the frazil ice density set to 950 kg m^{-3} [*Martin and Kauffman*, 1981] and L_s is the latent heat of formation of ice ($L_s \approx 235$ k J kg^{-1}), calculated following *Haarpaintner et al.* [2001]. If Q_{net} is negative, the water body transfers heat to the atmosphere and frazil ice is produced. The atmospheric forcing is assumed to be uniform over both the open water and thin ice regions. Finally, u in (1) is the speed of consolidated new ice at the open water edge (Figure 2).

[13] After formation, frazil ice instantaneously piles up against the open water edge and consolidates into a thin ice layer with thickness H. In this study, we determine H, following *Biggs et al.* [2000], as a function of the depth of frazil ice arriving at the open water edge and an increase in thickness caused by the piling up of frazil ice against ice floes.

[14] According to *Skogseth et al.* [2004], the drift of consolidated new ice away from the open water edge, u, can be described by

$$u = \epsilon_c U_a \cos(\varphi_m - \varphi_o), \quad (3)$$

where ϵ_c is a nondimensional proportionality constant, U_a is the wind speed and φ_m is the wind direction. Following *Pease* [1987], the constant of proportionality is set to 0.03. φ_o is is the wind direction with strongest effect on the opening of the polynya [*Haarpaintner et al.*, 2001]. The opening of the WNS polynya is most effective when the ice drift is normal to the fast ice boundary. The fast ice between the Lena Delta and the New Siberian Islands is aligned with about 50°, and according to Envisat satellite scenes, the ice drift differs about 10° to the right of the wind direction. Consequently, φ_o in (3) is set to 130°.

[15] The continuous thermodynamic growth of the consolidated new ice is calculated by Stefan's law [*Petrich and Eicken*, 2010]. In this study we apply the numeric equation of *Maykut* [1985] that considers an insulating snow layer on top of the ice, with the volumetric latent heat of freezing (L) set to 295.8 kJ kg^{-1} (note the difference from L_s used in (2)) and an ice density set to 920 kg m^{-3}. In spite of its simplicity, the so-called degree day model is capable of producing fairly accurate predictions of sea ice growth.

[16] The evolution of the pack ice edge P is reconstructed by a second drift equation

$$P_t = P_{t-\Delta_t} + U\Delta_t, \quad (4)$$

where P_t is the pack ice extent at time t and U is the velocity of the pack ice drift. U is calculated similar to equation (3), but with ϵ_c set to 0.01. The variability in ice drift between 1% of the wind velocity in very dense pack ice and 3% inside the polynya area is based on a comparison between the displacement of individual ice floes in SAR scenes and the wind velocity.

[17] The width of the thin ice zone I is calculated as the difference between P and R. The area of the polynya is computed by multiplying its width times the alongshore length of the WNS polynya (195 km).

[18] The accuracy of ice production estimates obtained from a polynya flux model was investigated by *Krumpen et al.* [2011a], who compared model results to ice thickness and ice production estimates derived from thermal infrared satellite data. It was found that regional discrepancies between model and satellite observations are at least partly due to the missing representation of the dynamics of thin ice thickening. To overcome this deficiency, we parameterize the effect of dynamic thickening of thin ice in the model by assuming that the differential drift of the pack ice and consolidated new ice, $U - u$, results in ice rafting and, therefore, compression of the thin ice zone, I. The dynamic ice thickening caused by this compression is governed by the equation of conservation of mass. Based on literature and field observations we assume rafting to be limited to ice thinner than 0.3 m [*Melling et al.*, 1993; *Worby et al.*, 1996; *Babko et al.*, 2002]. There is a lack of studies on rafting probabilities in thin ice, and so it is not known how the compression is distributed through ice thinner than 0.3 m. However, for simplicity, we assume the effects of compression on a thin ice zone to decrease linearly with ice thickness.

[19] As ice grows, salt is rejected and added to the water body. The amount of salt rejected is dependent on the initial surface salinity. The instantaneous salt flux from frazil ice growth in the open water zone, S_R, is calculated following *Winsor and Bjoerk* [2000] by assuming a spontaneous rejection of 69%. Once frazil ice consolidates to a thin solid layer, the formulation of *Ryvlin* [1974] is used to estimate salt rejection induced by the continuous growth of consolidated ice, S_I. For the 2008 event, a growth rate coefficient of 0.5 is applied, owing to comparatively high air temperatures. In contrast, the simulation of the comparatively cold 2004 event requires a lower value of 0.35. Note that the *Ryvlin* [1974] formula gives rather large salt entrapment for

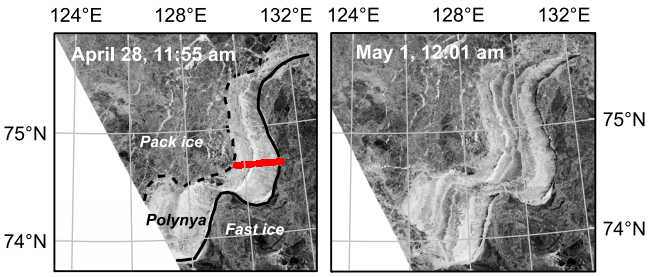

Figure 3. Envisat synthetic aperture radar (SAR) images acquired on (left) 28 April and (right) 1 May 2008, covering the WNS polynya. The sea ice regime consists of the fast ice zone (south of the black solid line), an active polynya zone (open water and thin ice), and a region of freely floating pack ice (north of the black dashed line). The red line in Figure 3 (left) highlights the profile of the helicopter-borne surveys of electromagnetic (HEM)-Bird ice thickness measurements on 29 April at 0400 UTC.

ice with thicknesses less than 10 cm compared to other empirical formula and observations. This might lead to a slight underestimation of salt rejection in the transition zone.

3. Data

3.1. Satellite Observations

[20] The evolution of the 2004 and 2008 polynya events were continuously monitored with different satellites.

[21] Envisat advanced SAR images provide information about ice dynamics in the eastern Laptev Sea. Each polynya event is covered by 4 scenes. Two of the scenes for 2008 and another two for 2004 are shown in Figures 3 and 4, respectively. The Envisat C band wide swath data is VV polarized and covers an area of approximately 400×800 km^2 with a spatial resolution of 150×150 m^2. Fast ice and pack ice edges, and hence the polynya width, are easily identifiable in SAR images. The determination of open water width is not straight forward, since the backscatter signatures inside the open water region and the consolidation zone can be very inhomogeneous and vary with meteorological conditions. In addition, often no clear boundary does exists between open water and consolidated thin ice. To validate open water width simulated by the model in 2008, the interpretation of Envisat SAR imagery is aided by helicopter-based observations, high-resolution TerraSAR-X scenes, meteorological data, and surface temperature information from the Advanced Very High Resolution Radiometer (AVHRR). The validation of the 2004 event simulation is exclusively based on Envisat SAR scenes, thermal AVHRR images and atmospheric information.

[22] The TerraSAR-X scenes (Strip Map Mode, X Band) are dual polarized (HH-VV) with a spatial resolution of 6.6×1.2 m^2 and cover a 15 km wide and 150 km long swath across the polynya. The 5 images were used to monitor thin ice dynamics and the evolution and width of the consolidation and open water zone during TD XIII. An example is given in Figure 5. A TerraSAR-X image obtained on 28 April 2008 at 0837 UTC is shown together with drift corrected aerial photographs, taken 3 h and 40 min before satellite acquisition. The three enlarged aerial photographs, with the black lines pointing to the corresponding footprint, show the open water zone (Figure 5a), the open water edge (Figure 5b), and rafted thin ice (Figure 5c).

[23] To validate the model simulated ice thickness, thermal infrared data is used to derive estimates of thermal ice thickness, h_{TH}, calculated with the aid of an atmospheric data set (section 3.4) using the surface energy balance model suggested by *Yu and Lindsay* [2003]. Ice surface temperatures (T_s) are derived from thermal infrared channels following the split window method of *Key et al.* [1997]. Level 1B calibrated radiances (visible and thermal infrared) were obtained from the U.S. National Oceanic and Administration (NOAA) Comprehensive Large Array data Stewardship System (CLASS). The spatial resolution of AVHRR Local Area Coverage (LAC) data is 1.1×1.1 km^2. The method requires clear sky conditions. In total, we identified 1 scene, covering the event in 2008, and 2 scenes imaging the opening in 2004. The thickness retrieval is based on the assumption that the heat flux through the ice equals the atmospheric heat flux. Following *Yu and Lindsay* [2003], h_{th} is inferred from the obtained T_s by

$$h_{th} = k_i(T_s - T_o)/Q_{net}, \tag{5}$$

where $T_o = -1.86$°C is the seawater temperature at freezing point and $k_i = 2.03$ W m^{-1} K^{-1} is the thermal conductivity of sea ice [*Drucker et al.*, 2003]. Q_{net} is calculated from equation (2), with same parameterizations as used for the model. The method yields good results for ice thicknesses below 0.5 m, further assuming that vertical temperature profiles within the ice are linear and no snow is present on top of the ice [*Drucker et al.*, 2003]. Figure 6 shows the thermal ice thickness distribution inside the polynya area as derived from an AVHRR image taken on 18 February 2004.

3.2. Airborne Data

[24] During TD XIII, two helicopter-borne surveys of electromagnetic (HEM) ice thickness, h_{HEM}, were performed across and along the WNS polynya. The profile obtained on 29 April 2008 is shown in Figure 3. It is used to validate polynya flux computations. The so-called EM-Bird, is an airborne electromagnetic (EM) system with a single frequency of 4.08 kHz [*Haas et al.*, 2009]. The instrument

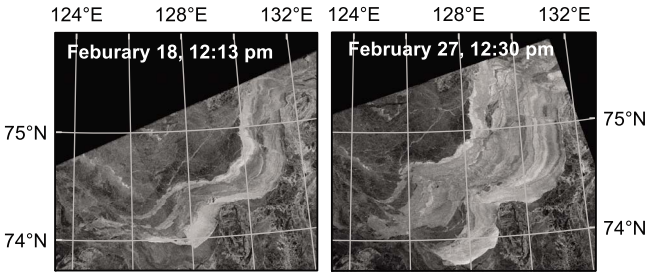

Figure 4. Envisat SAR images acquired on 18 and 27 February 2004. The scenes cover the position of the WNS polynya, showing the fast ice belt, the active polynya zone, and a region of freely floating pack ice.

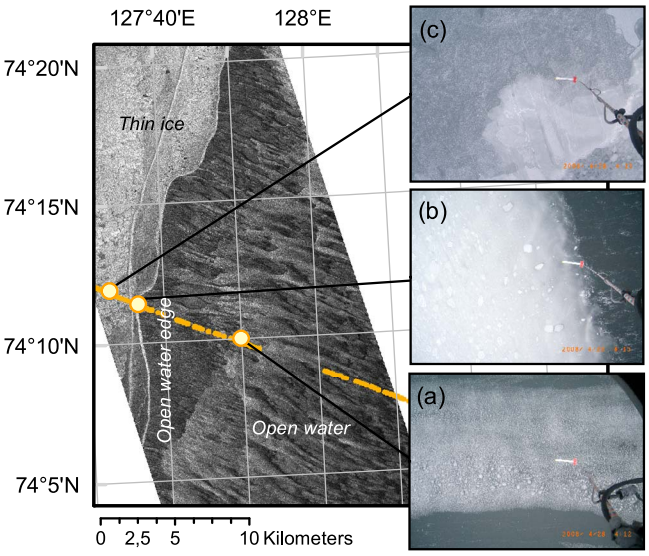

Figure 5. TerraSAR-X SAR image acquired on 28 April 2008 at 0837 UTC. The scene covers parts of the open water and thin ice zones of the WNS polynya. Aerial photographs taken on a helicopter flight across the polynya are plotted on top of the SAR scene as orange dots. The three enlarged aerial photographs, with the black lines pointing to the corresponding footprint, show (a) the open water zone, (b) the open water edge, and (c) rafted thin ice. In this study TerraSAR-X scenes were used to validate model simulated polynya evolution and ice dynamics and to aid the interpretation of Envisat SAR imagery.

was towed by a helicopter 15 meters above the ice surface. The method utilizes the contrast of electrical conductivity between seawater and sea ice to determine the distance to the ice-water interface. An additional laser altimeter yields the distance to the uppermost reflecting surface, hence h_{HEM} is obtained as the ice plus snow thickness from the difference between the laser range and the EM-derived distance. Since the laser beam is always reflected at the uppermost surface, snow thickness, if present, is included in h_{HEM}. However, the polynya event in 2008 is characterized by the absence of a snow cover on the thin ice, and therefore h_{HEM} presents the real ice thickness. The measurements were taken with point spacing of 3 to 4 m depending on the speed of the helicopter. Within the footprint of a single measurement (40–50 m) the accuracy over level sea ice is on the order of ±10 cm [*Pfaffling et al.*, 2007; *Haas et al.*, 2009].

[25] On all HEM flights, geocoded aerial photographs were taken with a downward-looking digital camera [*Krumpen et al.*, 2011b]. Images were used to provide general information about ice dynamics, to support the calibration of HEM ice thickness measurements and to aid TerraSAR-X and Envisat image interpretation (Figure 5).

3.3. Historical Hydrographic Information

[26] The mean stratification of the water column in winter 2004 was constructed by using salinity records obtained during the Arctic and Antarctic Research Institute (ARRI) Sever expeditions (1979–1990, 1992, and 1993), together with CTD measurements made during several Russian-German winter expeditions. The mean stratification pattern and its standard deviation (STDV) is calculated by averaging salinity measurements made in the center of the WNS polynya area during winter surveys, preconditioned by summers with a cyclonic atmospheric circulation regime. In total, 10 stations completed between February and May in the region of the WNS polynya are used to calculate the mean stratification pattern. Most of the surveys were carried out in the 70s and 80s, when the atmospheric circulation in summer was predominantly cyclonic [*Dmitrenko et al.*, 2009]. For a detailed description of the hydrographic data set we refer to the publication of *Dmitrenko et al.* [2009].

3.4. Atmospheric Data Set

[27] The model is driven with atmospheric data extracted from a single grid point in the center of the polynya. Polynya evolution, ice production and salt rejection are calculated using sea level pressure, 2 m air temperature and humidity, precipitation, surface net radiation and 10 m wind vectors.

[28] The simulation of the opening event of 2008 is driven with 1 hourly data from Consortium for Small-Scale Modeling (COSMO) simulations which were specifically performed for the Laptev Sea area by *Schroeder et al.* [2011]. By prescribing the polynya areas daily these data account for the impact of polynyas on the atmospheric boundary layer. The quality of the COSMO data is shown by a comparison with automatic weather stations and surface temperature derived from MODIS satellite data [*Schroeder et al.*, 2011].

[29] Ice and salt fluxes during the polynya event of 2004 are computed with 6 h National Centers for Environmental

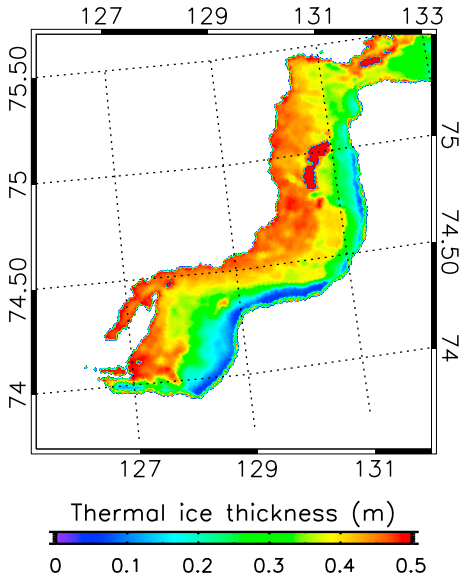

Figure 6. Thermal ice thickness (h_{TH}) as derived from Advanced Very High Resolution Radiometer (AVHRR) surface temperatures taken on 18 February 2004 at 1200 UTC and National Centers for Environmental Prediction (NCEP)/Department of Energy reanalysis data.

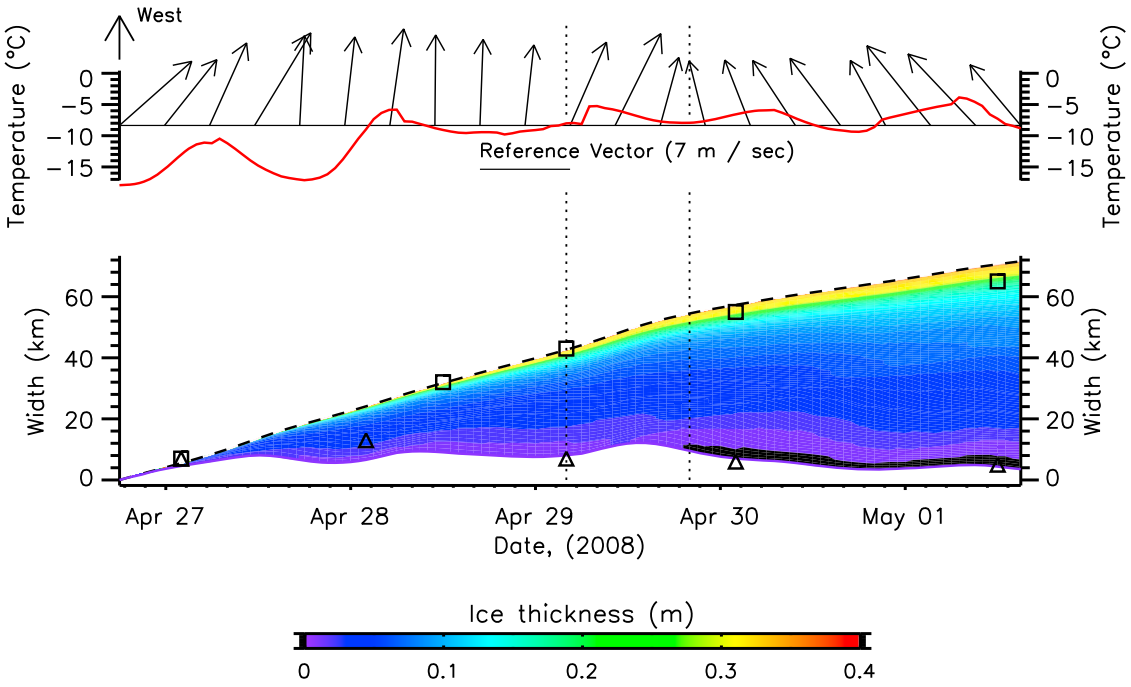

Figure 7. Atmospheric data (Consortium for Small-Scale Modeling) and polynya model results during the study period in April 2008. (top) Here 2 m air temperatures and 10 m wind vectors show the direction of air flow, with their lengths representing wind speed. (bottom) Modeled (black dashed line) and observed (black rectangles) total polynya width. Modeled ice thickness is color coded. The white area is the simulated open water width and the black triangles represent the observed open water width. Dotted vertical lines mark the dates of ice thickness reference measurements (HEM-Bird, 29 April at 0400 UTC; AVHRR, 29 April at 2000 UTC) used for model verification.

Prediction (NCEP)/Department of Energy (DOE) reanalysis atmospheric forcing fields [*Kanamitsu et al.*, 2002].

4. Model Simulations

4.1. Satellite Observations and Atmospheric Conditions During the 2008 Event

[30] According to airborne observations, AVHRR scenes and TerraSAR-X and Envisat SAR imagery, the 2008 polynya event started on 27 April and lasted for a period of 6 days. Consistent offshore winds and temperatures between −17°C and −4°C led to the formation of a 4–16 km wide open water zone and an extensive region of new thin ice. On 2 May air temperatures raised above the freezing point of seawater, causing the polynya to gain heat and ice production to halt.

[31] The COSMO-based 1 hourly air temperatures and 6 hourly wind velocities for the time of interest are presented in Figure 7 (top). Figure 3 shows the WNS polynya as observed by two SAR scenes acquired on 28 April and 1 May 2008. Open water zones are made visible by the brighter parallel wind-generated Langmuir streaks oriented perpendicular to the fast ice edge [*Drucker et al.*, 2003]. The bright and dark radar backscatter features within the polynya region are associated with pancake and frazil ice formation [*Kwok et al.*, 2007]. Several bands of consolidated new thin ice orientated nearly parallel to the fast ice edge are apparent downwind of the open water area.

4.2. Simulation of the 2008 Event

[32] The polynya flux model was used to simulate the first 5.25 days of the 2008 polynya opening event. The model's atmospheric forcing was extracted from the COSMO atmospheric data set. The salinity of the surface layer at the onset of the polynya opening was set to 26, following hydrographic observations made along the fast ice edge during TD XIII [*Dmitrenko et al.*, 2010b].

[33] Figure 7 (bottom) presents the simulated and observed (Envisat, TerraSAR-X and aerial photographs) evolution of the widths of the open water and thin ice areas, and the modeled thin ice thickness over the 5.25 days of simulation. At the onset of the polynya event, constant easterly winds push the pack ice edge offshore, resulting in the development of a wide open water zone. A thin ice zone in the model develops, and is then continuously thickening by thermodynamic and dynamic processes. On 29 April, the modeled thin ice zone extends up to 40 km offshore and the open water area reaches a width of approximately 8 km. Later, a slight change in wind direction and a temporary decrease in wind velocity cause a slow down of ice offshore transport, reducing the width of the open water zone to 4 km.

[34] The simulated evolution of the WNS polynya agrees well with observations. The mean deviation between mod-

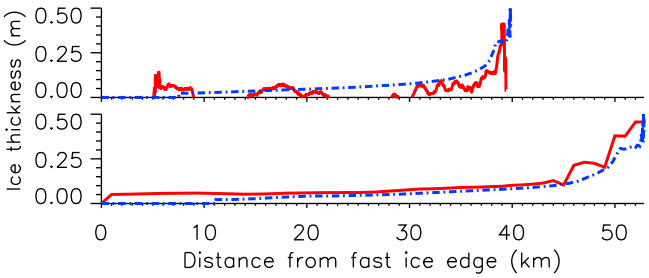

Figure 8. (top) Comparison of the HEM-Bird ice thickness profile (solid red line) taken on 29 April 2008 at 0400 UTC across the thin ice zone with the modeled ice thickness profile (dashed blue line). (bottom) Comparison of an AVHRR-derived ice thickness profile (h_{TH}, solid red line, 29 April 2008 at 2000 UTC) of the thin ice zone with the simulated ice thickness profile (dashed blue line).

eled and satellite observed position of the pack ice edge is 0.5 km. The deviation between modeled open water width and satellite and airborne observations is 1.4 km.

[35] The accuracy of the simulated thin ice thickness is tested by comparing model results to ice thickness estimates obtained from the HEM flight on 29 April at 0400 UTC and from a thermal infrared AVHRR scene acquired 14 h later (Figure 8). For comparison, HEM measurements were averaged over a 250 m interval. Gaps in h_{HEM} data at distances of 9–14 km and 23–26 km offshore the fast ice edge are the result of HEM instrument calibration [*Pfaffling et al.*, 2007]. The comparison shows that simulated ice thickness is near the range of h_{HEM} measurements, although the model overestimate the observations. Highest ice thicknesses can be found close to the pack ice edge in both HEM observations and model simulations.

[36] The agreement between AVHRR infrared ice thickness and model results is higher than between HEM measurements and model. Note that the AVHRR ice thickness profile shown in Figure 8 is averaged along the polynya. Both AVHRR and model data show an increase in ice thickness with distance from the fast ice edge. The simulated ice thickness tends to be generally lower than thermal ice thickness observations. As opposed to the model, the AVHRR sensor does not resolve the open water zone. Instead, the zone close to the fast ice edge is characterized by very low thicknesses varying between 0.01 and 0.05 m.

[37] In total, an ice volume of 1.4 km^3 is formed between 27 April and 1 May 2008. Of this ice, 40% (≈0.6 km^3) is produced in the open water zone, which represents on average 19% of the entire polynya area. The total amount of salt rejected is about 0.17×10^{11} kg, of which 0.1×10^{11} kg are rejected as frazil ice forms in open water zone. Putting our frazil ice–induced salt rejection estimates in relation to the mean seasonal salt rejection calculations made by Winsor and Bjoerk [2000] (0.77×10^{11} kg) the early spring polynya event accounts for approximately 13% of the mean seasonal salt flux. Distributing the amount of salt rejected in the open water zone with a mean width of 6.6 km over a no stratified water body with a depth of 25 m would result in a salinity increase of approximately 0.3.

4.3. Discussion of Flux Model Parameterizations and Performance

[38] Because ice production and salt rejection are highest in the open water area, accurate determination of the open water edge in the model is of paramount importance. The comparison of simulated open water width with observations made by helicopter, high-resolution TerraSAR-X scenes and Envisat SAR images has shown that the flux model is capable of simulating correctly the extend of the open water zone (Figure 7). This is in agreement with findings made by *Haarpaintner et al.* [2001], *Skogseth et al.* [2004], and *Krumpen et al.* [2011a]. Deviations between simulated and observed open water widths are related to the parameterizations and representation of physical processes in the model, and are discussed below.

[39] The assumption of spatial uniformity is justified by the fact that longshore variations in wind direction and air temperature, and their associated errors in computed ice and salt fluxes, are comparatively small for both polynya events. Nevertheless, if dealing with larger longshore polynya dimensions, the use of a two-dimensional flux approach driven by a spatially variable atmospheric forcing is required [*Krumpen et al.*, 2011a]. Note that in contrast to the NCEP/DOE reanalysis data used for the simulation of the 2004 event, the COSMO data set incorporates the impact of the polynya on the atmospheric boundary layer. T. Ernsdorf et al. (Impact of atmospheric forcing data on simulations of the Laptev Sea polynya dynamics using the sea-ice ocean model fesom, submitted to *Journal of Geophysical Research*, 2010) investigate the differences in ice production that result from the use of different atmospheric forcing data. Following Ernsdorf et al. (submitted manuscript, 2010), NCEP/DOE data overestimate temperatures by as much as 1.7 K, while COSMO is in good agreement with observations.

[40] A shortcoming of the polynya flux model is that frazil ice is assumed to instantaneously pile up against the thin ice edge. The incorporation of a finite frazil ice drift rate [*Ou*, 1988; *Biggs et al.*, 2000] and the effect of currents on the modeled frazil ice drift trajectories [*Willmott et al.*, 1997] becomes important as the open water region grows in size. However, the development of large open water zones in the eastern Laptev Sea polynyas is generally a rare event owing to prevailing low temperatures and moderate wind speeds during winter [*Winsor and Bjoerk*, 2000].

[41] We find the simulated open water region width and thin ice thickness to be extremely sensitive to the parameterization of the collection depth H. Different parameterizations used in one-dimensional and two-dimensional polynya flux models are discussed by *Martin and Kauffman* [1981], *Pease* [1987], *Alam and Curry* [1998], *Winsor and Bjoerk* [2000], *Morales Maqueda and Willmott* [2000], and *Krumpen et al.* [2011a]. Figure 9 shows how the simulated open water width differs if using different parameterizations of the collection depth. The use of a constant thickness parameterization (0.1 m or 0.2 m) as suggested by, e.g., *Pease* [1987] or *Haarpaintner et al.* [2001] leads to a crude overestimation of the width of the open water region. Most realistic results are achieved with the parameterizations developed by *Martin and Kauffman* [1981], [*Alam and Curry* [1998], and *Biggs et al.* [2000]. The work of *Martin and*

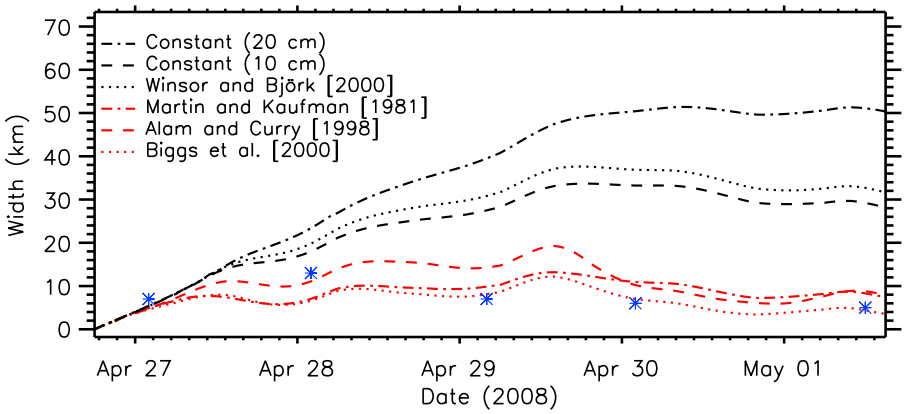

Figure 9. Open water width evolution during the 2008 poylyna event as calculated using different parameterizations for H. The blue stars represent the observed width of the open water zone.

Kauffman [1981] is based on laboratory observations showing that frazil ice accumulates with a thickness of 5–8 cm. Following *Martin and Kauffman* [1981], the frazil ice has an ice volume fraction of about 40%, such that H becomes 2–3 cm. *Alam and Curry* [1998] proposed an empirical parameterization that includes both wave and pressure effects. In this parameterization, the pile up thickness depends on both wind speed [*Winsor and Bjoerk*, 2000] and polynya width. The dependence on polynya width (or fetch) is an indirect way of taking into account wave radiation. When the polynya is too narrow, the wavefield is very weak and wave radiation cannot greatly influence pile up. As the polynya widens, the wavefield fully develops and wave radiation increasingly contributes to pile up. In our study, the best results were achieved by using the parameterization of *Biggs et al.* [2000], who determine the consolidation thickness as the sum of the thickness of frazil ice arriving at the edge and a pile up depth. In an earlier study we could show that, in addition to a more correct representation of the open water extent, the use of this parameterization results in most realistic thin ice thicknesses [*Krumpen et al.*, 2011a].

[42] The HEM- and AVHRR-derived thin ice thickness profiles and the model simulation show a thickness anomaly 5 km near the pack ice edge (Figure 8). This strong increase is too steep to result solely from thermodynamic growth, but is a consequence of enhanced dynamic thickening at the pack ice edge: In the model, the compression of the thin ice zone results from the difference in pack ice drift U and consolidated new ice velocity u. At the onset of the event, compression acts on a relatively narrow thin ice zone, resulting in a strong dynamic ice thickening and the development of the thickness anomaly in Figure 8. When the polynya widens and thin ice zone is growing in width, compression is distributed over a larger area and ice deformation weakens. The good agreement between observations and simulations indicates that the representation of dynamic ice growth in the model is a reasonable approximation. However, the drift equation for u is highly simplified and contains empirically tuned and uncertain parameters (equation (3)). Owing to the plasticity of the thin ice cover, ice drift rates are likely to vary in space and time. The associated ice production error is investigated in section 4.7.

[43] Note that the HEM profiles used to verify model results are challenging for two reasons. First, the processing of the EM-Bird data is based on the assumption that sea ice can be regarded as a nonconductive medium. Over thin ice, however, this assumption may be invalid because the conductivity of saline young ice can be significantly higher than that of older first-year or multiyear ice. This may lead to underestimates of the ice thickness. Therefore, all h_{HEM} data have to be interpreted as minimum ice thicknesses. Secondly, the conductivity of the surface waters can be low and highly variable due to their proximity to the freshwater input by the Lena River. Although a relatively low water conductivity of between 2200 and 2400 S m^{-1} was used for the retrieval of ice thicknesses, our processing algorithms do not take into account conductivity variations during individual flights.

[44] The accuracy of thermal infrared AVHRR thickness estimates is difficult to assess but believed to be within a range of ±20% [*Drucker et al.*, 2003]. Because time of interest is characterized by the absence of snow coverage, the largest source of error in h_{TH} probably arises from uncertainties in the atmospheric data set. Unfortunately, AVHRR thermal thickness estimates do not resolve open water zones present on SAR imagery and aerial photography. This is because in thermal infrared observations open water areas are characterized by a surface temperature close to the freezing point of seawater. Hence, the presence of frazil ice, Langmuir streaks or ice floes in the water column lowers the averaged surface temperature within the sensor footprint beneath freezing point, such that potential open water areas are classified as very thin ice.

4.4. Satellite Observations and Atmospheric Conditions During the 2004 Event

[45] According to the Envisat SAR scenes, the polynya event in 2004 started on 10 February, and remained open for 27 days. Strong and consistent offshore winds, together with extremely low air temperatures of between −44°C and −22°C, resulted in strong ice formation and the development of a broad open water area. Figure 10 (top) presents 6 hourly air temperatures and wind velocities taken from NCEP/DOE reanalysis data extracted from a single point nominally in

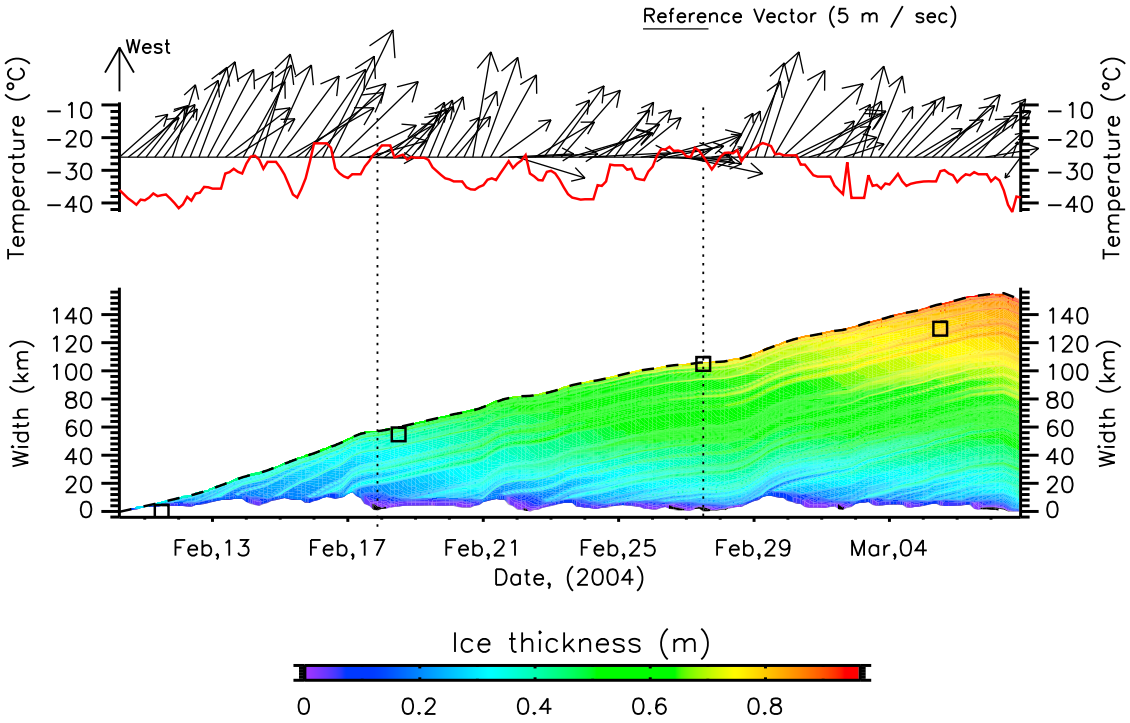

Figure 10. Atmospheric data (NCEP) and polynya model results during the study period in February 2004. (top) Here 2 m air temperatures and 10 m wind vectors show the direction of air flow, with their lengths representing wind speed. (bottom) Simulated (black dashed line) and observed (black rectangles) total polynya width. Simulated ice thickness is color coded. The white area is the simulated open water width. Dotted vertical lines mark the dates of ice thickness reference measurements (h_{TH}, AVHRR thermal infrared ice thickness estimates for 18 and 27 February 2004).

the center of the polynya. Figure 4 shows two SAR images taken on 18 and 27 February 2004. The polynya opened in a northwest direction. The thin ice zone grew up to an extent of approximately 140 km. A sudden change in wind direction on 5 March, caused a temporary closure of the polynya. As in Figure 3, the presence of Langmuir streaks indicates ice production in extensive open water zones. The banded structures orientated parallel to the polynya edge are located in the thin ice region.

4.5. Simulation of the 2004 Event

[46] We applied the polynya flux model to the simulation of the exceptionally strong polynya event in 2004. The evolution of the open water and thin ice zones, and the associated ice production and salt rejection, were calculated with atmospheric forcing extracted from NCEP/DOE reanalysis data.

[47] Figure 10 (bottom) presents the simulated and observed evolution of the extents of the open water and thin ice regions, as well as the modeled thin ice thickness over the 27 day duration of the polynya event. The simulated drift of the outer pack ice edge slightly overestimates the remotely sensed drift. A validation of the computed open water width is difficult with Envisat SAR images alone.

[48] Low air temperatures and high wind velocities (Figure 10, top), result in an enhanced thermodynamic and dynamic growth of the thin ice zone compared to the 2008 event. To evaluate the accuracy of the simulated thin ice thickness, we again compare AVHRR infrared ice thickness observations with the model results (Figure 11). The agreement between thermal ice thickness profiles taken on 18 and 27 February and simulations is high for areas 10 km offshore the fast ice edge. Further onshore, AVHRR estimates differ significantly from the ice thicknesses simulated by the flux model. The mean thin ice thickness on 18 February is 0.34 m for AVHRR and 0.38 m for model ice thickness. The respective thin ice thicknesses on 27 February are 0.32 m and 0.37 m.

[49] We estimate that, between 10 February and 5 March 2004, an ice volume of 26 km^3 was produced. Approximately 8.1 km^3 (32% of the total ice production) originates from frazil ice growth in the open water zone. This is

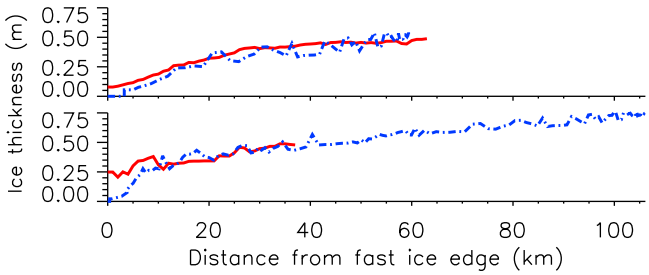

Figure 11. Comparison of AVHRR-based ice thickness profile (h_{TH}, solid red line) of the thin ice zone with the simulated ice thickness profile (dashed blue line) for (top) 18 and (bottom) 27 February 2004.

Table 1. Results of a Sensitivity Study Summarizing the Influence of Uncertainties Associated to Various Parameters on the Total Amount of Ice Formed in the Thin Ice Area and Open Water Area, as Well as the Ice Growth Rate Inside the Open Water Area Only

		Ice Production Error (%)		
Parameter	Variation	Thin Ice Area	Open Water Area	Ice Growth Rate
Air temperature (T_a)	±3°C	±6	±5	±9
Wind velocity (U_a)	±0.5 m s^{-1}	±8	±13	±5
Consolidated new ice velocity (ϵ_c)	±1%	±12	±35	±0
Collection depth (H)	±20%	±6	±18	±0
Cloud cover	±2/8	±0	±1	±1
Snow cover	±1 mm d^{-1}	±3	±0	±0
Ice thickness range affected by rafting	±0.1 m	±1	±0	±0

equivalent to 8 m ice production per unit area. A comparison of our calculations with annual polynya ice production estimates made by *Dethleff et al.* [1998], *Winsor and Bjoerk* [2000], and *Dmitrenko et al.* [2005] can be used as an indicator to check whether the 2004 event is a comparatively strong or a rather week event. According to *Winsor and Bjoerk* [2000], the annual ice formation in the area around the WNS polynya amounts to 14.2 m. If compared to estimates of *Winsor and Bjoerk* [2000], the 2004 event would contribute with as much as 57% to the mean annual ice production. *Dethleff et al.* [1998] calculated the flaw polynya to produce about 7.4 m of ice in winter 1991/1992, while the average annual polynya ice production calculated by *Dmitrenko et al.* [2005] is lower (3–4 m). If compared with these annual estimates, the 2004 event is an exceptionally strong one.

4.6. Discussion of the 2004 Event Simulation

[50] The simulated evolution of the pack ice edge is in good agreement with satellite observations. Unfortunately, a validation of the simulated open water width is difficult, as the edge of the open water region is not easily identifiable in SAR scenes. We have confidence, however, in our simulation of the open water evolution, as it was proven to be acceptably accurate for the well documented 2008 event. An additional indication of the degree of accuracy of the model can be derived from a comparison of the average length of Langmuir streaks in SAR images with the simulated open water width. A comparison shows that the model simulated open water width is in the range of Langmuir-based estimates. However, the accuracy of the SAR-based open water extraction very much depends on the image geometry (e.g., incident angle and spatial resolution) and atmospheric conditions (e.g., wind velocity). Hence, comparing Langmuir streak lengths with model results is a rather qualitative approximation for the model accuracy and therefore not shown here.

[51] The good agreement between simulated thin ice thickness and AVHRR-based estimates in areas 10 km offshore the fast ice indicates that the algorithms to calculate the ice drift rates U and u are well tuned. It also suggests that the parameterization for H calculated following *Biggs et al.* [2000], the applied approach to simulate thermodynamic ice growth and the dynamic thickening of thin ice are appropriate. The large discrepancies in ice thickness estimates near the fast ice edge eventually arise from the low spatial resolution of the AVHRR sensor compared to the polynya width. AVHRR-based water width estimates suffer from mixed pixel signatures, the presence of frazil ice, Langmuir streaks or ice floes in the water column that lower the averaged surface temperature within the sensor footprint beneath freezing point, such that potential open water areas are classified as very thin ice [*Willmes et al.*, 2010; *Krumpen et al.*, 2011a]. An additional uncertainty in the h_{TH} estimates arises from the potential presence of snow on the thin ice. The magnitude of this source of error is unknown. However, sensitivity tests made by *Yu and Rothrock* [1996] suggests that an uncertainty of 1 cm in snow depth results in a h_{TH} error greater than 100% for ice less than 5 cm thick and more than 50% for ice around 10 cm thick; this error decreases to about 33% for ice 20 cm thick and to 7% for ice 100 cm thick.

4.7. Sensitivity Study

[52] The evolution of the open water area and the amount of frazil ice being formed is most relevant for the ability of the polynya to erode the density stratification of the water body. Below we test how uncertainties associated to the parameterizations used in the 2004 computation would affect the ice growth rate inside the open water area, as well as the total amount of ice formed in the thin ice and open water zone. The results of this sensitivity study are summarized in Table 1.

[53] The presence of open water inside a closed ice pack gradually warms the air above. Because air temperatures for the 2004 event were taken from 6 h NCEP/DOE reanalysis data, where the impact of polynyas and leads is not considered, ice production rates are likely to be overestimated (Ernsdorf et al., submitted manuscript, 2010). Assuming the average air temperature in the area of the polynya to be 3°C lower/higher, causes the accumulated ice production inside the thin ice area to differ by ±6%. Likewise, the total ice production inside the open water zone varies by ±5%. The ice growth per unit area in the open water zone differs by ±9%. An average uncertainty in wind velocity of ±0.5 m s^{-1} would influence the ice volume produced in the thin ice and open water area by as much as ±8% and ±13%, respectively. The error associated to the ice production per unit area in the open water zone is less than the error associated to uncertainties in air temperatures (±5%).

[54] Other important parameters that determine the ice partition are the frazil ice collection depth (H) and the velocities of the ice edges (pack ice edge and open water edge, ϵ_c). According to satellite observations made in the area north of the fast ice edge, the evolution of the outer pack ice edge is well described by assuming it to be 1% of the wind speed. However, the determination of the consolidated new ice velocity (ϵ_c = 3%) is highly parameterized and might change in space and time. We therefore varied ϵ_c at the open water edge by a factor of ±1%. This significantly alters the evolution of the open water width. Consequently, the associated error in ice production is higher for the open water zone (±35%) than for the thin ice zone (±12%). The ice production per unit area in the open water zone is not affected. Varying the parameterization for the collection

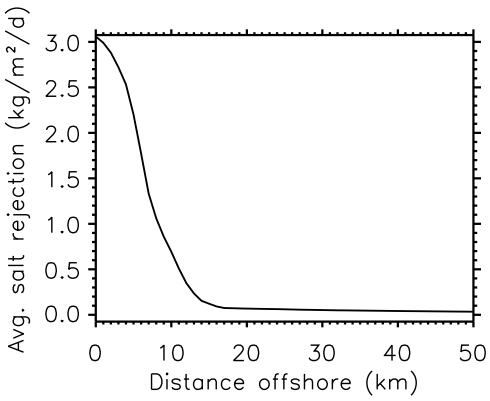

Figure 12. The average daily salt rejection (kg m^{-2} d^{-1}) during the 2004 polynya event as a function of distance offshore from the fast ice edge (km).

depth (H) calculated after *Biggs et al.* [2000] by ±20% results in an ice formation variation of ±6% in the thin ice zone and ±18% in the open water zone. Again, the ice growth rate in the open water zone does not change.

[55] The presence of a snow cover on young ice significantly reduces its growth rate. Varying the daily snow accumulation in the model by ±1 mm d^{-1} results in a thin ice production error of ±3%. If varying the cloud cover by a factor of ±2/8,the ice production in the open water area and ice growth per unit area deviate by ±1%. Note that the thermodynamic formulation of the thin ice growth used in our model is rather simplified and does not include, e.g., wind depended sensible heat fluxes. Hence, the computed total thin ice production is not affected by a varying cloud cover.

[56] The dynamical formulation used in our model is based on the assumption of convergent ice flow between the open water edge and the outer pack ice edge. The ice thickening is governed by the equation of conservation of mass by assuming rafting to be limited to ice thinner than 0.3 m and effects of compression on the thin ice zone to decrease linearly with ice thickness. The error associated to this highly idealized parameterization is tested by limiting rafting in a separate model run to ice classes thinner than 0.2 and 0.4 m. However, the resultant variation of ice growth in the thin ice zone was found to be negligibly small (±1%).

[57] The algorithms used to calculate heat flux, ice growth and salt rejection are based upon several empirical coefficients. An evaluation of the errors associated to the use of specific coefficients such as the bulk transfer coefficient or L_s is beyond the scope of this study. At this point the authors refer to the publication of *Haarpaintner et al.* [2001], where this topic is covered in more detail.

5. Effect of Ice Formation on the Water Column Stratification

[58] The total amount of salt rejected during the polynya event in 2004 was estimated at about 2.9×10^{11} kg, of which 1.5×10^{11} kg were rejected in the open water area as frazil ice was created. Figure 12 shows the daily averaged salt rejection as a function of distance offshore from the fast ice edge. Highest rates are released during frazil ice formation in areas near the fast ice edge, while fluxes related to the thermodynamic growth of consolidated new ice further offshore are significantly lower.

[59] If the amount of salt released and subsequent dense brine rejected is high enough, the stratification of the shelf may be temporarily eroded. Locally confined haline convection cells may then lead to the formation of dense shelf bottom water that accumulates over the shelf and eventually flows down the shelf break slope to form deep water [*Backhaus et al.*, 1997]. *Chapman and Gawarkiewicz* [1997] and *Chapman* [1999] examined shallow convection and offshore transport of dense water from an idealized coastal polynya using a theoretical approach. Model results suggest that a baroclinically unstable front developes at the edge of the polynya. Dense water is then formed and transported offshore in baroclinic eddies that develop along this front. The role of polynyas in forming and disseminating saline waters over the central Bering shelf was further investigated by *Danielson et al.* [2006] using 14 yearlong moorings deployed south of St. Lawrence Island. In contrast to the theoretical prediction of *Chapman and Gawarkiewicz* [1997] and *Chapman* [1999], *Danielson et al.* [2006] found negligible cross-shelf eddy density fluxes within and surrounding shallow polynyas even though dense water accumulated within the polynya and large cross-shore density gradients developed. The hydrographic response to the polynya activity in the southeastern Laptev Sea was recently investigated by [*Dmitrenko et al.*, 2010b]. However, similar to *Danielson et al.* [2006] the authors found no baroclinic instability and eddy formation along the fast ice edge, although the thermohaline front across the onshore polynya boundary was highly pronounced.

[60] At present, the oceanographic processes contributing to density-driven convection and formation of dense bottom water on the southeastern Laptev Sea shelf are not fully understood. To examine whether density-driven convection during a strong polynya event penetrates to the bottom, we therefore neglect any horizontal advection of dense water in our investigation. In this study, the impact of salt rejection on the stratification of the water body is investigated by uniformly distributing the rejected salt (Figure 12) over a stagnant water body. Information on mean winter stratification and its standard deviation preconditioned by cyclonic summers are derived from historical hydrographic data (section 3.3). Figure 13 shows the mean winter stratification of the water column and its STDV before and after the polynya event. Neglecting any currents, release of brines from freezing sea ice convectively erodes the pronounced seasonal halocline near the fast ice edge down to a depth of 30 m (Figure 13, middle). Further offshore (5 and 10 km) the convection depth is limited to 25 and 13 m water depth, respectively. If instead of the mean winter stratification, we use the mean winter stratification plus its STDV (Figure 13, left), the shelf stratification can be fully mixed within a 5 km distance from the fast ice edge. If we subtract, rather than add, the STDV to the mean winter stratification (Figure 13, right) the density-driven convective mixing depth is significantly reduced. Areas near the fast ice edge are eroded down to a depth of 22 m. Further offshore, mixing is limited to 16 m (5 km offshore) and 10 m (10 km offshore) water depth. To test if the penetration depth varies throughout the polynya area, we averaged hydrographic measurements made

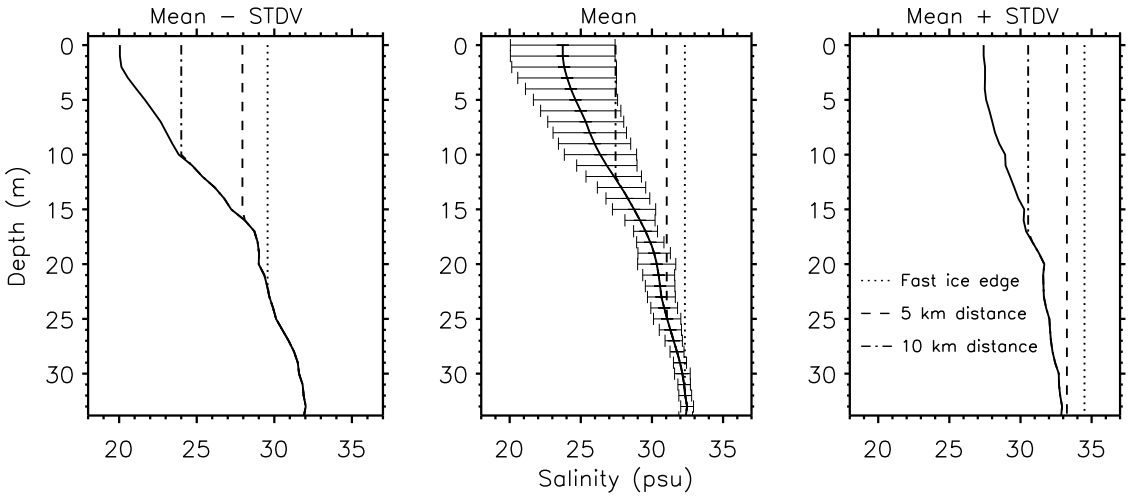

Figure 13. Effect of salt rejection on the stratification of the water body. (middle) The mean water layer stratification for winters preconditioned by summers with a cyclonic atmospheric forcing (solid line). Error bars denote the standard deviation (STDV) from mean. Information on mean stratification and its variance is computed from the historical hydrographic data. The dotted, dashed, and dash-dotted lines represent the simulated salinity increase near the fast ice edge and 5 and 10 km offshore. (left and right) The mean stratification ±STDV and the polynya-induced modification of the layer stratification at different distances from the fast ice edge.

further north and south of the polynya center. However, the obtained climatological mean stratification patterns are very similar to the mean stratification pattern at the polynya center (not shown here). Consequently, the convective mixing depths computed on the basis of mean stratification patterns are consistent throughout the polynya area.

[61] The use of a mean climatological stratification plus/minus its STDV to investigate if the water body gets fully eroded during strong polynya events is admittedly somewhat crude. The approach is merely exploratory, but sufficiently rigorous, we expect, to provide a zero-order estimate of the potential contribution of polynya events to winter destratification. The mixed layer depths we report on in the previous paragraph may probably be considered as upper bound estimates of destratification potential, as in our simulations, destratification is favored in a number of ways that we enumerate in the following.

[62] First, the sensitivity study has shown that largest errors in ice growth rates per unit area are associated to uncertainties in air temperatures. In the 2004 event simulation we applied a NCEP/DOE atmospheric data set that was shown to generally underestimate air temperatures owing to the missing incorporation of the impact of polynyas on the atmospheric data set (Ernsdorf et al., submitted manuscript, 2010). The incomplete representation of polynya processes results in an overestimation of polynya ice production, and consequently an overestimation of salt rejection rates. Second, as pointed out in section 5.2, the simulated polynya event was exceptionally consistent with extreme ice formation and salt rejection rates. Third, the climatological mean density stratification used in this study to investigate the impact of ice production on the water stratification was calculated by averaging salinity measurements made during winter surveys preconditioned for destratification by cyclonic summers. In addition, the calculated mean stratification may contain profiles that were taken during active polynya events and/or have been weakened by preceding polynya activity. However, indentifying those profiles to exclude them from the calculation is not possible, since potential polynya activity has not always been documented. Note that most of the profiles were obtained in the 70s and 80s, when the spatial resolution of satellites was too coarse to resolve single polynya events. We therefore expect the strength of the mean vertical density gradient to be underestimated, rather than overestimated.

[63] Figure 14 shows a series of single hydrographic measurements that were taken along and offshore the fast ice edge during the TD VI expedition in April 1999. Following *Dmitrenko et al.* [2005], the summer of 1998 was predominantly cyclonic with the third highest vorticity index observed since 1948. By the time measurements were made, the WNS polynya was closed. Note that compared to the climatological mean stratification, the profiles shown in Figure 14 are characterized by a much stronger density gradient. Figure 14 shows the potential effect of the 2004 polynya event on the water body, if the amount of salt released is integrated over the stratification of stations 1, 2, and 3. The deepest level of penetration is achieved at station 1, located at the southern edge of the WNS polynya. Neglecting any currents, the stratification of the water body near the fast ice edge is fully mixed. In the center of the polynya (station 3), the strength of the pycnocline is more pronounced. As a consequence, a cross-pycnocline mixing is prevented and penetration depth is limited to the upper 13 m. Following *Chapman and Gawarkiewicz* [1997], one could argue that baroclinic eddies eventually transport dense water formed in open water zones offshore to areas with a less distinct density gradient. Here, mixing may occur localized in chimneys or eddies. However, according to *Dmitrenko et al.* [2010b], the entire central part of the southeastern Laptev Sea is of generally low surface salinity. For example, station 2 in Figure 14 shows the stratification that was

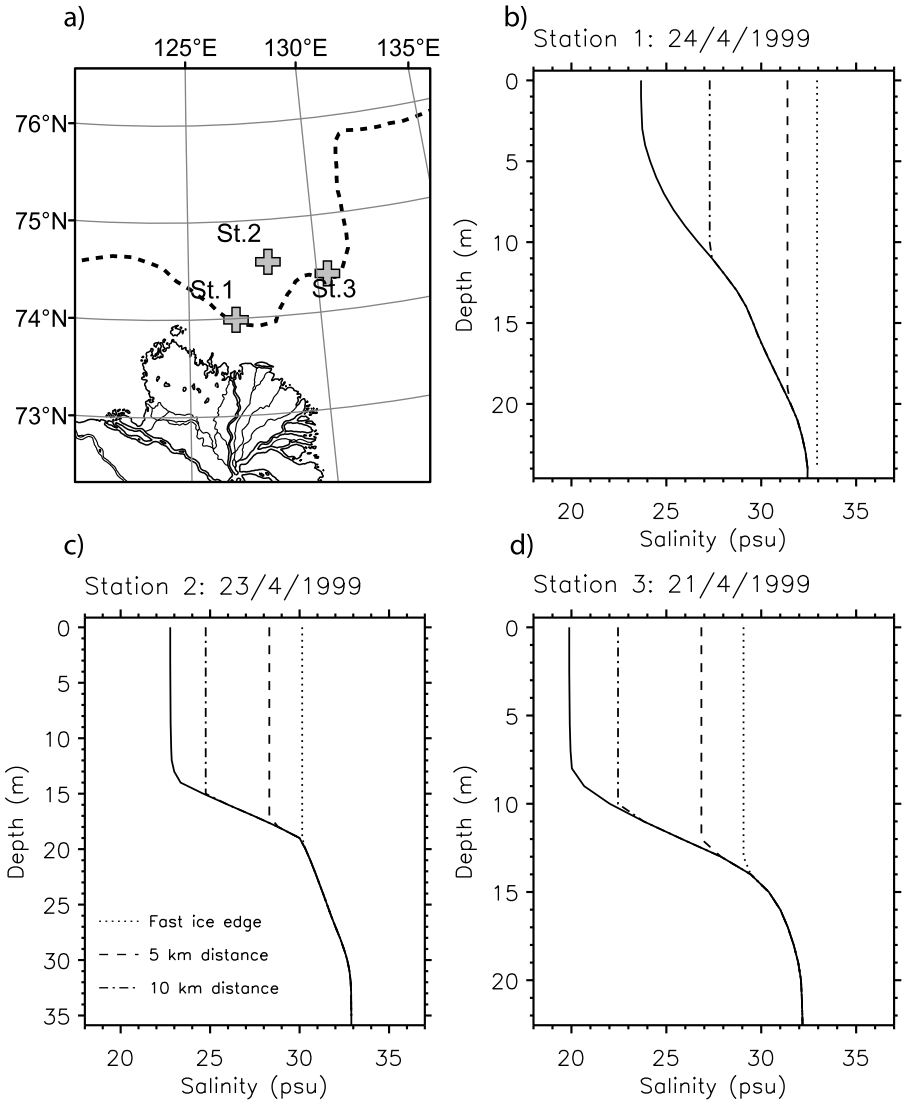

Figure 14. Effect of salt rejection on the stratification of the water body as observed at three different stations during TD VI in April 1999. (a) The southeastern Laptev Sea, the location of the fast ice edge in April 1999 (dashed line) and positions were oceanographic profiles were taken (crosses). The observed water layer stratification at stations (b) 1, (c) 2, and (d) 3 are shown. Like in Figure 13 the dotted, dashed, and dash-dotted lines represent the simulated salinity increase with distance from fast ice edge.

observed during TD VI, approximately 40 km offshore from the fast ice edge. The strength of the pycnocline is as pronounced as at station 3, such that mixing is limited to the upper 20 m water depth.

[64] Our assumption of a stagnant water body neglects the background current flow that eventually brings water of different salinity to the WNS polynya. If the water origins from under the fast ice, as it was the case during TD VI, it advects less saline water into the area of ice formation, and thus helps to restore stratification. An inclusion of these advective processes in the model would further strengthen the stability of the water column and would prevent density-driven convection to penetrate down to the bottom. In contrast, the likelihood for deep mixing is increased, if an alongshore advection establish that brings water of higher salinity from the Anabar or Taimyr polynya (Figure 1) into the polynya area. Theoretically, this alongshore flow may even further increase its salinity while crossing the polynya from southwest to northeast.

[65] Recent year-round mooring observations made during the period from September 2007 until September 2009 in the region of the WNS polynya provide evidence that active polynya formation is usually accompanied by a sharp decrease in near-bottom water salinity and temperature [*Hölemann et al.*, 2011]. These observations are inconsistent with dense water formation by brine rejection and support our assumption that even during strong WNS polynya events, ice production is not high enough to erode the halocline. *Hölemann et al.* [2011] suggest that the salinity decrease is likely to be induced by a wind driven breakdown of the stratification and a cross-pycnocline turbulent mixing, leading to an admixture of the brine enriched but still buoyant surface waters to the more saline, and denser bottom waters (>25 m water depth). Up to know, vertical

transport of heat and matter on shelf seas are believed to be controlled by both turbulent and convective mixing [*Schauer*, 1995; *Rippeth*, 2008; *Dethleff*, 2010]. However, our results provide indirect evidence that the mechanisms responsible for the destratification and vertical mixing in the area around the WNS polynya are predominantly wind- and tidally driven, rather than convective. This has far-reaching consequences for both the vertical and lateral distribution of nutrient, sediments, pollutants and heat.

6. Conclusions

[66] In this study, we investigate the ice formation that took place during an exceptionally strong and consistent WNS polynya event in 2004. We further examine whether associated salt rejection rates are high enough to establish a density-driven convection that penetrates down to the bottom of the seafloor. Ice production rates were computed by means of a simple polynya model driven by standard atmospheric forcing. The effect of salt rejection on the water body is examined by adding the brine released during the polynya event to the average winter density stratification of the water body preconditioned by summers with a cyclonic atmospheric forcing. The model performance was also tested by applying it to the simulation of a well documented WNS polynya event in April 2008.

[67] The simulation of the opening event in 2008 shows that the model is capable of reproducing correctly the extent of the open water zone and the location of the pack ice edge. The good agreement between the simulated thickness of the thin ice zone and estimates made by airborne surveys and AVHRR satellite indicates that the model is well tuned, and suggests that the approach is a suitable tool to investigate the dynamics and export rates of flaw polynyas.

[68] Applying the model to the strong polynya event in 2004, results in a total ice volume production of 26 km^3. This corresponds to a brine release of 2.9×10^{11} kg. Neglecting the replenishment of water masses by advection into the polynya area, the probability for the occurrence of density-driven convection down to the bottom is low. This can be explained by the distinct density gradient that characterize the area of the WNS polynya and the apparent lack of extreme events in the eastern Laptev Sea. The simple approach is expected to be sufficiently rigorous, since ice production and salt rejection rates are likely to be overestimated owing to the incomplete representation of polynya processes in the atmospheric data set. Furthermore, the simulated event is exceptionally consistent with extreme ice formation and salt rejection rates and the strength of the climatological mean stratification pattern is likely to be underestimated, rather than overestimated. Our findings are supported by mooring-based observations in the WNS polynya that show that large polynya openings are usually associated with a decrease in near-bottom water salinity and temperature at water depth greater than 25 m, which is predominantly related to wind- and tidally driven turbulent mixing of the water column. This (the absence of convective mixing down to the seabed and subsequent dense water formation) has far-reaching consequences on the today's understanding of energy and matter transport on the eastern Laptev Sea shelf.

[69] Understanding how the stratification of shallow shelf water and the ice production and salt rejection in polynyas might change in a warming climate is one of the major challenges of current polar research. On the one hand, it is likely, that the stability of the halocline will be strengthened by an increase in the Siberian river discharge [*Bethke et al.*, 2006; *Peterson et al.*, 2006]. Rising Arctic surface temperatures [*Chapman and Walsh*, 2007] will probably weaken ice production and increase summer sea ice melt, further promoting the stability of the halocline. On the other hand, the observed positive trend in summer cyclonicity over the Eurasian Arctic [*Simmonds et al.*, 2008; *Simmonds and Keay*, 2009] might destabilize the water column (change the water column structure). Likewise, a decrease in ice production could be compensated by an increase in polynya activity during the freeze up period and in early spring [*Willmes et al.*, 2011] caused by an increase in the frequency and strength of cyclones penetrating into the Eurasian Arctic [*Zhang et al.*, 2004].

[70] Clearly, we are far from being able to formulate sound predictions of how polynya formation and water column stratification will respond to climatic change. Understanding and quantifying this response are key tasks for future shelf process studies. To draw inferences on the physical behavior of polynyas, under the premise that the climate in the Arctic is changing, a numerical approach is needed. Nevertheless, our results show that an alteration of mechanisms responsible for vertical mixing in the WNS polynya would require a strong increase in ice production and/or a significant weakening of the year-round density stratification.

[71] **Acknowledgments.** This work was carried out as part of the German-Russian cooperation "System Laptev Sea," funded by the BMBF under grant 03G0639A and the Alfred Wegener Institute. Envisat satellite data and AVHRR images were obtained through ESA Project EO-500 "Formation, transport and distribution of sediment-laden sea ice in the Arctic Shelf seas" and the U.S. National Oceanic and Administration (NOAA) Comprehesive Large Array data Stewardship System (CLASS), respectively. Thanks to the Arctic and Antarctic Research Institute (AARI) for the provision of the hydrographic data set, the German Aerospace Center (DLR) for the provision of the TerraSAR-X imagery (grand COA0388), and the German Federal Ministry of Economics and Technology (BMWi) for their support. The authors also very much appreciate numerous helpful comments and suggestions made by Sönke Maus from the GFI, University Bergen, and Sergey Kirillov from the AARI.

References

Aagaard, K., J. H. Swift, and E. C. Carmack (1985), Thermohaline circulation in the Arctic Mediterranean seas, *J. Geophys. Res.*, *90*, 4833–4846.

Alam, A., and J. A. Curry (1998), Evolution of new ice and turbulent fluxes over freezing winter leads, *J. Geophys. Res.*, *103*, 15,783–15,802.

Babko, O., D. A. Rothrock, and G. A. Maykut (2002), Role of rafting in the mechanical redistribution of sea ice thickness, *J. Geophys. Res.*, *107*(C8), 3113, doi:10.1029/1999JC000190.

Backhaus, J. A., H. Fohrmann, J. Kaempf, and A. Rubina (1997), Formation and export of water masses produced in Arctic shelf polynyas—Process studies of oceanic convection, *J. Mar. Sci.*, *54*, 366–382.

Barber, D. G., and R. A. Massom (2007), The role of sea ice in Arctic and Antarctic polynyas, in *Polynyas: Windows to the World*, *Elsevier Oceanogr. Ser.*, vol. 74, edited by W. O. Smith Jr. and D. G. Barber, pp. 1–54, chap. 1, Elsevier, Amsterdam.

Barber, D. G., J. J. Yackel, and J. M. Hanesiak (2001), Sea ice, RADARSAT-1 and Artic climate processes: A review and update, *Can. J. Remote Sens.*, *16*, 51–61.

Bethke, I., T. Furevik, and H. Drange (2006), Towards a more saline North Atlantic and a fresher Arctic under global warming, *Geophys. Res. Lett.*, *33*, L21712, doi:10.1029/2006GL027264.

Biggs, N. R. T., M. A. Morales Maqueda, and A. J. Willmott (2000), Polynya flux model solutions incorporating a parameterisation for the collection thickness of consolidated new ice, *J. Fluid Mech.*, *408*, 179–204.

Cavalieri, D. J., and S. Martin (1994), The contribution of Alaskan, Siberian, and Canadian coastal polynyas to the cold halocline layer of the Artic Ocean, *J. Geophys. Res.*, *99*, 18,343–18,362.

Chapman, D. (1999), Dense water formation benearth a time-dependent coastal polynya, *J. Phys. Oceanogr.*, *29*, 807–820.

Chapman, D., and G. Gawarkiewicz (1997), Shallow convection and buoyancy equilibration in an idealized coastal polynya, *J. Phys. Oceanogr.*, *27*, 555–566.

Chapman, W. M., and J. E. Walsh (2007), Simulations of Arctic temperature and pressure by global coupled models, *J. Clim.*, *20*, 609–632.

Danielson, S., K. Aagaard, T. Weingartner, S. Martin, G. Winsor, P. Gawarkiewicz, and D. Quadfasel (2006), The St. Lawrence polynya and the Bering shelf circulation: New observations and a model comparison, *J. Geophys. Res.*, *111*, C09023, doi:10.1029/2005JC003268.

Dethleff, D. (2010), Dense water formation in the Laptev Sea flaw lead, *J. Geophys. Res.*, *115*, C12022, doi:10.1029/2009JC006080.

Dethleff, D., P. Loewe, and E. Kline (1998), The Laptev Sea flaw lead—Detailed investigation on ice formation and export during 1991/1992 winter season, *Cold Reg. Sci. Technol.*, *27*, 225–243.

Dmitrenko, I. A., K. N. Tyshko, S. A. Kirillov, H. Eicken, J. A. Hölemann, and H. Kassens (2005), Impact of flaw polynyas on the hydrography of the Laptev Sea, *Global Planet. Change*, *48*, 9–27.

Dmitrenko, I. A., S. A. Kirillov, and B. L. Tremblay (2008), The long-term and interannual variability of summer fresh water storage over the eastern Siberian shelf: Implication for climatic change, *J. Geophys. Res.*, *113*, C03007, doi:10.1029/2007JC004304.

Dmitrenko, I. A., S. A. Kirillov, L. B. Tremblay, D. Bauch, and S. Willmes (2009), Sea-ice production over the Laptev Sea shelf inferred from historical summer-to-winter hydrographic observations of 1960s–1990s, *Geophys. Res. Lett.*, *36*, L13605, doi:10.1029/2009GL038775.

Dmitrenko, I. A., S. A. Kirillov, T. Krumpen, J. A. Hölemann, H. Kassens, M. Makhotin, P. Abrahamsen, E. Bloshkina, and C. Wegner (2010a), Wind-driven diversion of summer river runoff preconditions the Laptev Sea coastal polynya hydrography: Evidence from summer-to-winter hydrographic records of 2007–2009, *Cont. Shelf Res.*, *30*, 1656–1664.

Dmitrenko, I. A., et al. (2010b), Observations of supercooling and frazil ice formation in the Laptev Sea coastal polynya, *J. Geophys. Res.*, *115*, C05015, doi:10.1029/2009JC005798.

Drucker, R., S. Martin, and R. Moritz (2003), Observation of ice thickness and frazil ice in the St. Lawrence Island polynya from satellite imagery, upward looking sonar, and salinity/temperature moorings, *J. Geophys. Res.*, *108*(C5), 3149, doi:10.1029/2001JC001213.

Gloersen, P., W. J. Campbell, D. J. Cavalieri, J. Comiso, and C. Parkinson (1992), *Arctic and Antarctic Sea-Ice*, 1978–1987*: Satellite Passive-Microwave Observations and Analysis*, NASA, Washington, D. C.

Haarpaintner, J., M. Haugan, and J. Gascard (2001), Interannual variability of the Storfjorden (Svalbard) ice cover and ice production observed by ERS-2 SAR, *Ann. Glaciol.*, *33*, 430–436.

Haas, C., J. Lobach, S. Hendricks, L. Rabenstein, and A. Pfaffling (2009), Helicopter-borne measurements of sea ice thickness, using a small and lightweight, digital EM system, *J. Appl. Geophys.*, *67*, 234–241.

Hölemann, J. A., S. Kirillov, T. Klagge, A. Novikhin, H. Kassens, and L. Timokhov (2011), Near-bottom water warming in the Laptev Sea in response to atmospheric and sea ice conditions in 2007, *Polar Res.*, doi:10.3402/polar.v30i0.6425, in press.

Ivanov, V. V., and P. N. Golovin (2007), Observations and modeling of dense water cascading from the northwestern Laptev Sea shelf, *J. Geophys. Res.*, *112*, C09003, doi:10.1029/2006JC003882.

Kanamitsu, M., W. Ebisuzaki, J. Woollen, S. K. Yang, J. J. Hnilo, M. Fiorino, and G. L. Potter (2002), NCEP-DOE AMIP-II Reanalysis (R-2), *Bull. Am. Meteorol. Soc.*, *83*, 1631–1643.

Key, J. R., J. B. Collins, C. Fowler, and R. S. Stone (1997), High-latitude surface temperature estimates from thermal satellite data, *Remote Sens. Environ.*, *61*, 302–309.

Krumpen, T., S. Willmes, M. A. Morales Maqueda, C. Haas, J. Hölemann, R. Gerdes, and D. Schroeder (2011a), Evaluation of a polynya flux model by means of thermal infrared satellite observations, *Ann. Glaciol.*, *52*, 52–60.

Krumpen, T., C. Haas, S. Hendricks, J. Hölemann, R. Gerdes, and D. Kalmbach (2011b), HELIOS, a nadir-looking sea ice monitoring camera, *Cold Reg. Sci. Technol.*, *65*, 308–313, doi:10.1016/j.coldregions.2010.11.007.

Kwok, R., J. C. Comiso, R. Martin, and S. Drucker (2007), Ross Sea polynyas: Response of ice concentration retrievals to large areas of thin ice, *J. Geophys. Res.*, *112*, C12012, doi:10.1029/2006JC003967.

Lebedev, V. L. (1968), Maximum size of a wind-generated lead during sea freezing, *Oceanology*, *8*, 313–318.

Lenn, Y. D., et al. (2008), Vertical mixing at intermediate depths in the Arctic boundary current, *Geophys. Res. Lett.*, *36*, L05601, doi:10.1029/2008GL036792.

Martin, S., and P. Kauffman (1981), A field and laboratory study of wave dumping by grease ice, *J. Glaciol.*, *27*, 283–313.

Maykut, G. A. (1985), *The Surface Heat and Mass Balance, The Geophysics of Sea Ice*, Martinus Nijhoff, Dordrecht, Netherlands.

Melling, H., D. R. Topham, and D. A. Riedel (1993), Topography of the upper and lower surfaces of 10 hectares of deformed sea ice, *Cold Reg. Sci. Technol.*, *21*, 349–369.

Morales Maqueda, M. A., and A. J. Willmott (2000), A two-dimensional time-dependend model of a wind-driven coastal polynya: Application to the St. Lawrence island polynya, *J. Phys. Oceanogr.*, *30*, 1281–1304.

Morales Maqueda, M. A., A. J. Willmot, and N. R. T. Biggs (2004), Polynya dynamics: A review of observation and modeling, *Rev. Geophys.*, *42*, RG1004, doi:10.1029/2002RG000116.

Ou, H. W. (1988), A time-dependent model of a coastal polynya, *J. Phys. Oceanogr.*, *18*, 584–590.

Pease, C. H. (1987), The size of wind-driven coastal polynyas, *J. Geophys. Res.*, *92*, 7049–7059.

Peterson, B. J., J. W. McClelland, R. Curry, R. M. Holmes, J. E. Walsh, and K. Aagaard (2006), Trajectory shifts in the Arctic and Subarctic freshwater cycle, *Science*, *313*, 1061–1066.

Petrich, C., and H. Eicken (2010), Growth, structure and properties of sea ice, in *Sea Ice*, 2 ed., edited by H. S. Dieckmann and H. Helmer, pp. 23–77, chap. 2, Wiley-Blackwell, Oxford, U. K.

Pfaffling, A., C. Haas, and J. E. Reid (2007), A direct helicopter EM sea ice thickness inversion, assessed with synthetic and field data, *Geophysics*, *72*, F127–F137.

Reimnitz, E., D. Dethleff, and D. Nuernberg (1994), Contrasts in Arctic shelf sea-ice regimes and some implications: Beaufort Sea and Laptev Sea, *Mar. Geol.*, *28*, 179–210.

Rippeth, T. P. (2008), Mixing in seasonally stratified shelf seas: a shifting paradigm, *Philos. Trans. R. Soc. A*, *363*, 2837–2854.

Ryvlin, A. I. (1974), Method of forecasting flexural strength of an ice cover (in Russian), *Probl. Arct. Antarct.*, *45*, 79–86.

Schauer, U. (1995), The release of brine-enriched shelf water from Storfjord into the Norwegian Sea, *J. Geophys. Res.*, *100*, 16,015–16,028.

Schauer, U., R. D. Muench, B. Rudels, and L. Timokhov (1997), Impact of eastern Arctic shelf waters on the Nansen Basin intermediate layers, *J. Geophys. Res.*, *102*, 3371–3382.

Schroeder, D., G. Heinemann, and S. Willmes (2011), Implementation of a thermodynamic sea ice module in the NWP model COSMO and its impact on simulations for the Laptev Sea area in the Siberian Arctic, *Polar Res.*, doi:10.3402/polar.v30i0.6334, in press.

Sherwood, C. R. (2000), Numerical model of frazil ice and suspended sediment concentrations and formation of sediment laden ice in the Kara Sea, *J. Geophys. Res.*, *105*, 9411–9422.

Simmonds, I., and K. Keay (2009), Extraordinary September Arctic sea ice reductions and their relationships with storm behavior over 1979–2008, *Geophys. Res. Lett.*, *36*, L19715, doi:10.1029/2009GL039810.

Simmonds, I., C. Burke, and K. Keay (2008), Arctic climate change as manifest in cyclone behavior, *J. Clim.*, *21*, 5777–5796.

Skogseth, R., P. M. Haugan, and J. Haarpaintner (2004), Ice and brine production in Storfjorden from four winters of satellite and in situ observations and modeling, *J. Geophys. Res.*, *109*, C10008, doi:10.1029/2004JC002384.

Smedsrud, L. H. (2004), Formation of turbid ice during autumn freeze-up in the Kara Sea, *Polar Res.*, *22*, 267–286.

Smith, S. D., R. D. Muench, and C. H. Pease (1990), Polynyas and leads: an overview of physical processes and environment, *J. Geophys. Res.*, *95*, 9461–9479.

Smith, W. H. F., and D. T. Sandwell (1997), Global seafloor topography from satellite altimetry and ship depth soundings, *Science*, *277*, 1957–1962.

Willmes, S., T. Krumpen, S. Adams, L. Rabenstein, C. Haas, J. Hoelemann, S. Hendricks, and G. Heinemann (2010), Cross-validation of polynya monitoring methods from multisensor satellite and airborne data: A case study from the Laptev Sea, *Can. J. Remote Sens.*, *36*, S196–S210.

Willmes, S., S. Adams, D. Schroeder, and G. Heinemann (2011), Spatio-temporal variability of polynya dynamics and ice production in the Laptev Sea between the winters of 1979/80 and 2007/08, *Polar Res.*, doi:10.3402/polar.v30i0.5971, in press.

Willmott, A. J., M. A. Morales Maqueda, and M. S. Darby (1997), A model for the influence of wind and oceanic currents on the size of a steady-state latent heat coastal polynya, *J. Phys. Oceanogr.*, *27*, 2256–2275.

Willmott, A. J., D. M. Holland, and M. A. M. Maqueda (2007), Polynya modeling, in *Polynyas: Windows to the World*, *Elsevier Oceanogr. Ser.*, vol. 74, edited by W. O. Smith Jr. and D. G. Barber, pp. 87–126, chap. 3, Elsevier, Amsterdam.

Winsor, P., and G. Bjoerk (2000), Polynya activity in the Artic Ocean from 1958 to 1997, *J. Geophys. Res.*, *105*, 8789–8803.

Worby, A. P., M. O. Jeffries, W. F. Weeks, K. Morris, and R. Jana (1996), The thickness distribution of sea ice and snow cover during late winter in the Bellingshausen and Amundsen seas, Antarctica, *J. Geophys. Res.*, *101*, 28,441–28,455.

Yu, Y., and R. Lindsay (2003), Comparison of thin ice thickness distributions derived from RADARSAT Geophysical Processor System and advanced very high resolution radiometer data sets, *J. Geophys. Res.*, *108*(C12), 3387, doi:10.1029/2002JC001319.

Yu, Y., and D. A. Rothrock (1996), Thin ice thickness from satellite thermal imagery, *J. Geophys. Res.*, *101*, 25,753–25,766.

Zakharov, V. F. (1966), The role of flaw leads off the edge of fast ice in the hydrological and ice regime of the Laptev Sea, *Oceanology*, *6*, 815–821.

Zhang, X., J. Walsh, U. Bhatt, and M. Ikeda (2004), Climatology and interannual variability of Arctic cyclone activity: 1948–2002, *J. Clim.*, *17*, 2300–2317.

T. Busche, Microwave and Radar Institute, German Aerospace Center, Münchner Str. 20, D-82234 Wesseling, Germany.

I. A. Dmitrenko and H. Kassens, Leibniz Institute of Marine Sciences, University of Kiel, Wischhofstr. 1-3, D-24148 Kiel, Germany.

R. Gerdes, S. Hendricks, and T. Krumpen, Department of Sea Ice Physics, Alfred Wegener Institute, Busse Str. 24, D-27570 Bremerhaven, Germany. (tkrumpen@awi.de)

C. Haas, Department of Earth and Atmospheric Sciences, University of Alberta, 1-26 Earth Sciences Bldg., Edmonton, AB T6G 2E3, Canada.

G. Heinemann, D. Schröder, and S. Willmes, Department of Environmental Meteorology, University of Trier, Behringstr. 21, D-54286 Trier, Germany.

J. A. Hölemann, Department of Observational Oceanography, Alfred Wegener Institute, Busse Str. 24, D-27570 Bremerhaven, Germany.

M. A. Morales Maqueda, National Oceanography Centre, 6 Brownlow St., Liverpool L3 5DA, UK.

L. Rabenstein, Institute of Geophysics, ETH Zurich, Sonneggstr. 5, CH-8092 Zurich, Switzerland.